Journal of
Ceramic Science
and Technology

J. Ceram. Sci. Technol., **08** [3] 377-388 (2017)
DOI: 10.4416/JCST2017-00047
available online at: http://www.ceramic-science.com

High-Temperature Behaviour of Alkali-Activated Composites based on Fly Ash and Recycled Refractory Particles

L. Carabba[1], S. Manzi[1], E. Rambaldi[2], G. Ridolfi[2], M.C. Bignozzi*[1, 2]

[1]Department of Civil, Chemical, Environmental and Materials Engineering, University of Bologna, via Terracini 28, Bologna, Italy
[2]Centro Ceramico, via Martelli 26, Bologna, Italy

received June 30, 2017; received in revised form July 17, 2017; accepted August 21, 2017

Abstract

This study aims to develop innovative and sustainable alkali-activated composites with enhanced performance at high temperatures. To reduce production costs and promote a circular economy model, coal fly ashes are selected as a precursor for the alkali activation and recycled refractory particles are used to develop products with high thermal dimensional stability. Matrices and composites are investigated as a function of two curing conditions (heat curing vs room temperature curing) and amounts of dispersed phase (recycled refractory particles) added to the matrix. Thermal stability is assessed based on thermal exposure in a muffle furnace at 800 and 1000 °C, heating microscope analysis, and dilatometry. In addition, mineralogical quantitative analyses are performed to obtain an insight into phase changing after thermal exposure. Results show that the recycled refractory particles do not hinder the alkali activation process, significantly reduce heat-induced cracking, increase the maximum temperature of dimensional stability of the composites up to 1240 °C, and improve the linear dimensional stability during heating. In addition, the heat curing does not significantly increase the temperature range of dimensional stability, whereas the room temperature curing generates a product less prone to cracking when exposed to high temperature, and therefore it can be preferred.

Keywords: Alkali-activated composites, fly ash, refractory, thermal behaviour, heat exposure

I. Introduction

Nowadays, alkali-activated materials (AAMs) are effectively considered a new toolkit in the development of a sustainable materials industry [1]. This technology is based on the reaction between a solid aluminosilicate source and an alkali activator to obtain a mainly amorphous 3D network of silicoaluminates with binding properties [2]. One of the main advantages of this new class of materials consists in the possibility of using waste powders such as slags and coal fly ashes as an amorphous aluminosilicate source [3], taking advantage of their reactivity in sodium and/or potassium hydroxide and silicate solutions. Currently, AAMs are mostly investigated as reduced-CO_2 construction materials as an alternative to Portland-based cements [4]. However, the wide variety of parameters involved in the process (e.g., raw materials, activators, curing conditions) allows tailoring of the mix design for applications in several different fields ranging from the development of high-tech composites to hazardous waste management [5].

One of the most interesting features of AAMs is their remarkable thermal stability owing to the intrinsic thermal resistance of their inorganic structure [5–7]. Most of the research on thermal behaviour of AAMs focuses on metakaolin (MK)-based systems because of the relatively pure oxide composition of this precursor. Results obtained so far show that the thermal behaviour of AAMs is sensitive to the Al/Si ratio and to the alkali activator chosen for the process [8, 9] and have revealed that, when properly designed and cured, MK-AAMs withstand up to 1300 °C without significant changes in their structure [7].

Unlike metakaolin, coal fly ash (FA) originates from waste streams and for this reason, its microstructure is much more complex, comprising a mixture of amorphous and crystalline components [10, 11]. Indeed, fly ash generally contains a significant proportion of impurities such as iron oxides, which have direct influence on the thermal expansion, the phase composition, and the morphology of the material after heating [12]. On the other hand, the use of fly ash provides multiple benefits for the environment [13, 14] and requires a lower amount of activators than metakaolin [15], which also means lower production costs for fly-ash-AAMs. Moreover, FA-AAMs are more permeable than MK-based systems. For high-temperature applications this feature has turned out advantageous because the vapour pressure generated by water evaporation can easily be dissipated without any damage/cracking of the matrix [16, 17]. However, because of the large variety in fly ash composition, the formulation of FA-AAMs often needs to be optimized in order to reach the required high thermal dimensional stability [18].

* Corresponding author: maria.bignozzi@unibo.it

Previous studies dealing with high-temperature exposure of alkali-activated composites showed that it is possible to improve their thermal behaviour by adding suitable fillers and/or reinforcing phases in the matrix. In particular, the good compatibility of aluminosilicate, α-alumina, wollastonite, chamotte, PVA, basalt particulates and fibers with alkali-activated matrices was assessed [19–24], confirming the possibility to overcome issues such as high shrinkage and changes in compressive and flexural strength caused by high-temperature exposure.

With the aim to go forward with the research on FA-AAMs, the present study investigates the possibility to use recycled refractory particles (RRP) to obtain fly-ash-based alkali-activated composites with enhanced thermal dimensional stability. The use of recycled materials as both precursor (fly ash) and reinforcement particles (RRP) potentially allows a reduction in the production costs and promotes a circular economy model. The influence of two curing conditions (heat curing vs room temperature curing) and RRP addition on the composite features was analysed. The thermal behaviour of fly-ash-alkali-activated matrices and composites was studied using heating microscope analysis, dilatometry and thermal exposure in a muffle furnace at 800 and 1000 °C. In addition, mineralogical quantitative analyses were performed to obtain an insight into phase changes after the thermal exposure.

II. Experimental

(1) Materials

In this study, coal fly ash (FA) was used as a precursor for the synthesis. The FA was sourced from the coal-fired power station of Torrevaldaliga Nord, Italy. The chemical composition (Table 1) had been investigated in previous studies [25,26] which classified this FA as suitable raw material for FA-AAM production.

Sodium hydroxide in pellets (supplied by Sigma-Aldrich) and sodium silicate solution (SiO_2/Na_2O ratio = 2.07, ϱ = 1.530 g/cm^3, kindly supplied by Ingessil Srl, Verona, Italy) were used as alkaline activators. Recycled aluminosilicate refractory particles (RRP) (d_{max} = 2 mm, kindly supplied by Keratech, Gorizia, Italy) obtained by milling industrial scraps of refractory roller production were used to enhance the thermal stability of the final product. In XRD analysis, RRP show a crystalline nature comprised of mullite, corundum and baddeleyite (Fig. 1), which is consistent with the chemical composition provided by the producer and reported in Table 1.

(2) Synthesis

Fly-ash alkali-activated matrices were synthesized with Si:Al and Na:Al compositional ratios of 2.9 and 0.9 – 1.0, respectively. The composites were obtained by adding the recycled refractory particles to the matrix in the amounts of 10, 20, 30, and 40 wt%. The addition of RRP caused a requirement for extra water to preserve the workability of the mixture. Therefore, the composites contain a total water content of 16.5 wt% by the total mass, calculated as the sum of extra water and the water coming from the solution.

Fly ash and refractory particles were pre-mixed in a Hobart mixer for 30 s, after which alkaline solutions were added together with extra water, when required. After 6 min of mixing, the mixer was paused for 60 s and then mixing was resumed for further 3 min. The slurry was poured into cylindrical (ø = 35 mm, h =20 mm) and prismatic (40 × 40 × 160 mm) moulds and compacted on a jolting table.

Table 1: Oxide composition of fly ash (FA) and recycled refractory particles (RRP).

Oxide	FA (wt%)	RRP (wt%)
SiO_2	49.4	17.0
Al_2O_3	29.2	78.0
Fe_2O_3	2.7	< 0.3
TiO_2	1.6	-
CaO	6.6	-
MgO	1.1	-
K_2O	0.6	-
SO_3	0.3	-
Other oxides (Na_2O, BaO, Cr_2O_3)	< 0.1	-
ZrO_2	-	4.7
LOI	3.3	-
Insoluble residue	5.1	-

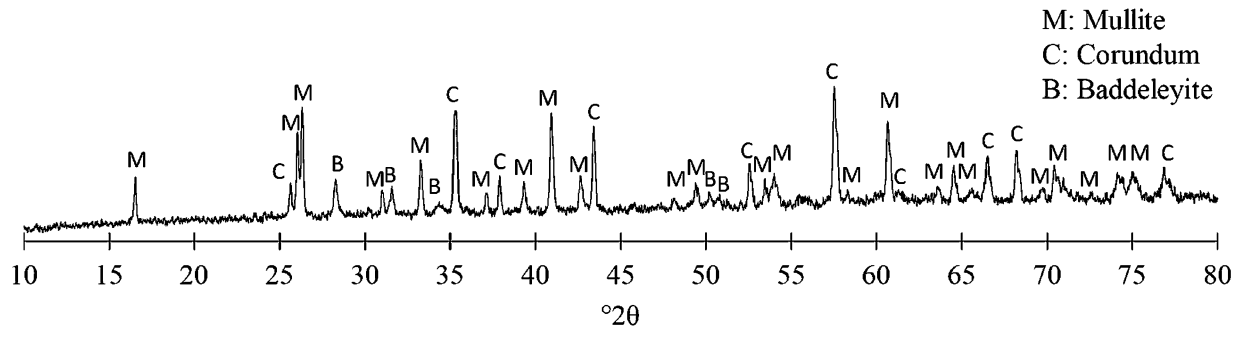

Fig. 1: X-ray pattern of the recycled refractory particles (RRP).

Two different curing processes were adopted for the first 24 h: heat curing (T = 70 ± 1 °C) and room temperature curing (T = 21 ± 2 °C). In both cases the moulds were sealed in plastic bags to prevent fast evaporation of the water. After the first 24 h, all the specimens were demoulded and cured sealed in plastic bags at room temperature for further six days. All the results presented in this study refer to the characterization of the specimens after seven days of curing.

Specimens are named according to the amount of the contained RRP expressed in weight percentage by the total mass and to the curing conditions adopted (T and A indicate heat curing and room temperature, respectively).

(3) Instruments and test methods

The quantitative mineralogical compositions of the samples were determined by means of X-ray diffraction analysis (PW3830, Philips, NL). Powdered specimens, diluted with 10 wt% rutile as internal standard, were side-loaded to minimize preferred orientation. Data were collected in the angular range 10 – 80° 2θ with steps of 0.02° and 5 s/step and the Rietveld refinements were performed using GSAS [27].

The bulk density (ϱ_{bulk}) of the cylinders was obtained by dividing the dry mass (after drying in an oven at 105 °C for 24 h) by the volume, which was calculated based on hydrostatic weighing. The same specimens were used for determining the water absorption (WA%), obtained by soaking dried cylinders for 24 h in water under vacuum conditions. Results are expressed as a percentage of the difference between the saturated surface-dried mass and the dry mass divided by the dry mass. An insight into the influence of the curing conditions on the pore size distribution of the matrix was obtained by means of mercury intrusion porosimetry (MIP, Carlo Erba 2000 instrument equipped with a macropore unit Model 120, Fison Instruments). Cubic specimens (40 × 40 × 40 mm) obtained from the prismatic specimens were used for measuring the compressive strength (Rc) in an Amsler-Wolpert machine at a constant displacement rate of 50 mm/min.

Thermal treatment in a muffle furnace was performed. The as-cured cylinders were heated at 5 K/min to the two set temperatures of 800 and 1000 °C, held at these temperatures for 2 h, and then allowed to cool naturally back to room temperature. Mass loss and changes in density and water absorption were measured as an average of two results.

A heating optical microscope (HSM, Expert System) was used with the aim of observing the behaviour of the product during heating. Samples measuring 3 × 3 × 5 mm were heated at a constant rate of 5 K/min until complete melting of the sample was achieved.

The linear dimensional variations were measured with a dilatometer 402 E, Netzsch GmbH. Prismatic samples measuring 5 × 9 × 25 mm were heated from ambient temperature up to 1000 °C at a constant rate of 10 K/min.

III. Results and Discussion

(1) Characterization of matrices

Mineralogical analysis of the matrices cured in the two different conditions (0_T and 0_A) are reported in Table 2. Results show a prevalent amorphous nature (amorphous phase content equal to 89.9 ± 2.0 and 87.3 ± 0.6 wt% in 0_T and 0_A, respectively) and small amounts of mullite and quartz as crystalline phases coming from the FA precursor. The two different curing conditions do not strongly influence the mineralogical nature of the material, thus in the following paragraphs only the room-temperature-cured samples (A-series) are described from the mineralogical point of view.

Mineralogical analysis was also performed on the 0_A sample after it had been exposed for 2 h to 800 °C (0_A_800) and 1000 °C (0_A_1000) in order to investigate the heat-induced changes in the mineralogical composition of the matrix (Table 2). The treatment at 800 °C causes a reduction of around 37.6 % in the amorphous phase content. Nepheline and plagioclase feldspar are formed as new crystalline phases and a slight decrease in the quartz and mullite content is observed. With the thermal treatment at 1000 °C, no other new phases are formed, but plagioclase feldspar content slightly increases compared to the previous treatment at 800 °C and amorphous phase slightly decreases. These two findings are correlated since it is highly probable that the new phases are the result of a crystallization of the amorphous aluminosilicate gel [28, 29]. Fig. 2 shows the pore size distributions of the matrices cured in the two different conditions (0_T and 0_A). The specific volume of mercury intruded in 0_T sample is higher than that in 0_A, indicating a higher total open porosity for the heat-cured sample. The dimensions and distribution of the pores change with the curing conditions as well. In the 0_T sample, the pore size distribution curve is shifted towards left, indicating the presence of smaller pores

Table 2: Mineralogical phase composition of the as-cured 0_T and 0_A samples and of the 0_A sample after thermal treatment at 800 and 1000 °C.

Phase content (wt%)	0_T	0_A	0_A_800	0_A_1000
Quartz	4.4±0.6	6.1±0.4	2.3±0.3	2.2±0.2
Mullite	5.7±0.3	6.6±0.6	5.0±0.8	5.4±0.8
Nepheline	-	-	4.5±0.8	4.9±0.6
Plagioclase feldspar	-	-	33.7±0.5	37.4±0.3
Amorphous phase	89.9±2.0	87.3±0.6	54.5±3.0	50.1±3.0

compared to 0_A. Moreover, the 0_T sample shows a unimodal distribution of pores in the range of 0.04 – 0.01 μm, whereas the sample cured at room temperature has pores distributed in the range of 0.5 – 0.004 μm. Even if the 0_A sample exhibits lower porosity than 0_T, the largest pore distribution strongly influences the mechanical properties. Indeed, 0_A exhibits a compressive strength of 11.3 ± 1.5 MPa, that is less than half of that showed by 0_T (25.8 ± 6.7 MPa). This behaviour was somehow expected since it is known that heat curing usually boosts the activation process, increasing the degree of reaction and therefore favouring the rapid development of a more resistant gel in terms of mechanical properties [30].

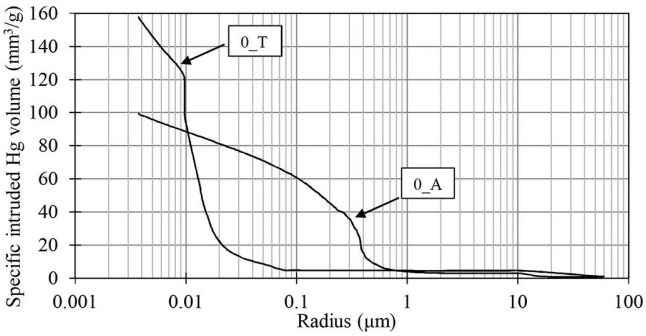

Fig. 2: Pore size distributions of the 0_T and 0_A samples after seven days of curing.

To give an insight into other high-temperature-induced modifications of the matrices, the quantification of mass loss, density and water absorption after thermal treatment are reported in Table 3 together with the bulk density and water absorption of the as-cured specimens and the mass loss measured after drying of the samples at 105 °C.

The total mass loss of 0_A is higher than that of 0_T on account of a slower water evaporation owing to the different curing conditions. Heating at 105 °C promotes sample dehydration, which can be considered as the major cause of weight decrease. Heating up to 800 °C causes a further mass loss connected to the additional dehydration of the bound water and to the dehydroxilation that occur in the temperature range of 105 – 400 °C [31]. This is more evident in the 0_T specimen, which experiences an additional mass loss of about 3 %, whereas the 0_A sample shows a negligible variation (1 %). These results are connected to the different curing conditions and the relevant different microstructures formed in 0_T and 0_A. In fact, generally in AAMs, water is mainly in the form of free water in large pores and bound water in small pores [32]. Therefore, the presence of large pores in the 0_A sample promotes higher mass loss values owing to the evaporation of free water, whereas the contribution of mass loss owing to the dehydration of the bound water is more evident for heat-cured samples. In the temperature range going from 800 °C to 1000 °C, both specimens can be considered stable, as variations < 1 % in the mass are observed.

The thermal treatment at 800 °C also causes an increase in density values and a decrease in the measured water absorption compared to the as-cured samples. This behaviour is likely related to a localised sintering process of the matrix gel [29]. The reduction of water absorption values, indicating a modification of the samples' open porosity, can also be related to the localised viscous sintering of the gel [33]. Indeed, it is possible that the viscous flow hinders the accessibility of the porosity, creating isolated pores which remain unfilled with water during the test. Conversely, when heated up to 1000 °C, the 0_A and 0_T samples show different behaviour. Further gradual densification occurs in the 0_A sample, whereas 0_T shows a decrease in density and an increase in water absorption. The anomalous behaviour determined for 0_T is due to the severe cracking (Section III (3)) of the sample with consequent volumetric expansion [29].

(2) Characterization of the composites

Composites prepared with different content of RRP (10, 20, 30, and 40 wt%) exhibit a homogeneous distribution of the particulate-dispersed phase (Fig. 3).

The mineralogical composition of the 30_A and 40_A samples (cured at room temperature) was analysed by means of quantitative XRD analysis, as representative samples. Corundum and traces of baddeleyite are detected as new crystalline phases characteristic of RRP. Compared to the matrix (0_A), a lower content of amorphous phase and an increased amount of mullite are determined, according to the different content of dispersed RPP. Amorphous phase proportionally decreases with the increase in the RRP content (Fig. 4), indicating that the RRP is neither reactive during the activation process nor hinders the process itself and can be effectively considered as inert in the process.

Table 3: Quantification of mass loss, density and water absorption of the matrices after drying (T = 105 °C) and thermal treatment (T = 800 and 1000 °C)

	0_A			0_T		
	105 °C	800 °C	1000 °C	105 °C	800 °C	1000 °C
Mass loss (%)	17.70±0.11	18.74±0.12	19.26±0.01	11.09±0.35	14.07±0.34	14.78±0.23
Density (g/cm³)	1.57±0.01	1.69±0.01	1.70±0.01	1.59±0.01	1.65±0.01	1.49±0.01
Water absorption (%)	21.55±0.29	15.98±0.08	10.87±0.63	22.19±0.16	17.52±0.35	21.77±1.14

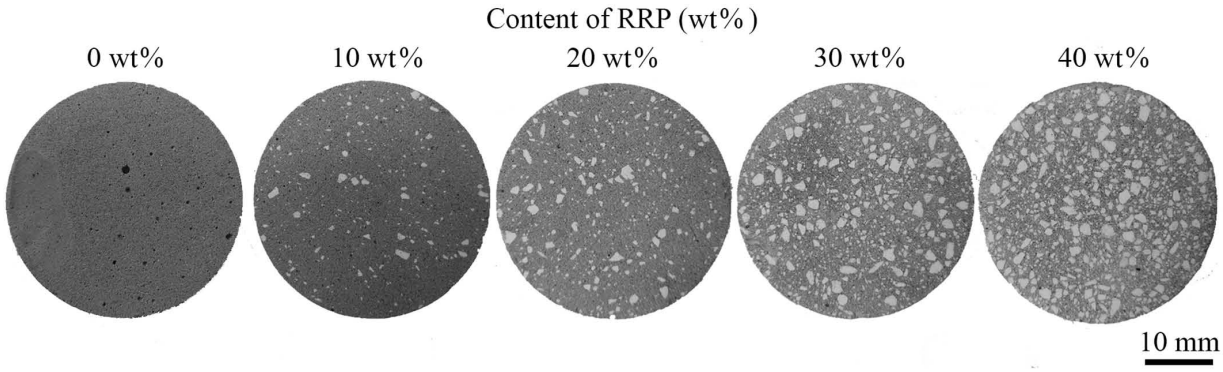

Fig. 3: Pictures of the as-cured specimens containing an increasing amount of RRP.

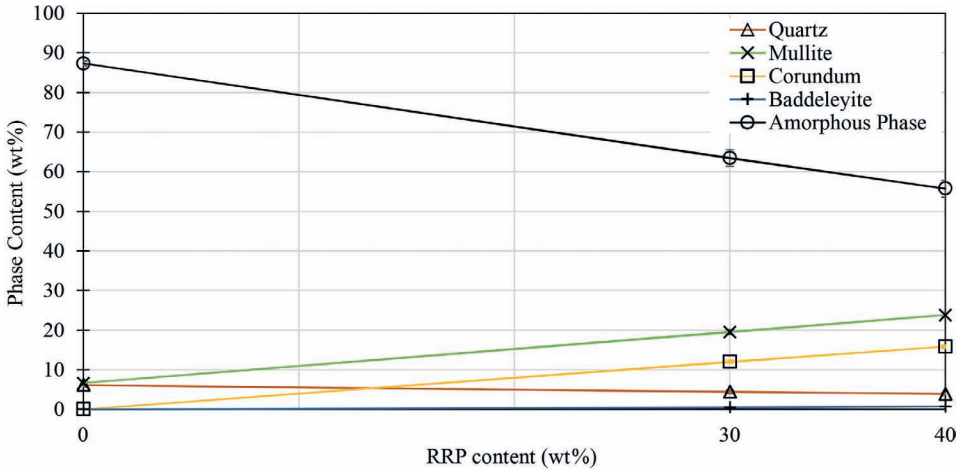

Fig. 4: Mineralogical phase composition of the as-cured 0_A, 30_A, and 40_A samples.

Table 4: Mineralogical phase composition of the30_A and 40_A samples before and after thermal treatment at 800 and 1000 °C.

Phase content (wt%)	30_A	30_A_800	30_A_1000	40_A	40_A_800	40_A_1000
Quartz	4.4±0.4	2.3±0.2	1.9±0.2	3.9±0.4	2.8±0.3	2.7±0.3
Mullite	19.5±0.6	24.2±0.6	24.9±0.5	23.8±0.6	33.3±0.6	33.2±0.6
Corundum	12.0±0.4	16.2±0.5	16.3±0.4	15.8±0.4	24.1±0.6	24.0±0.5
Baddeleyite	Trace (<1)	0.7±0.2	Trace (<1)	Trace (<1)	Trace (<1)	Trace (<1)
Nepheline	-	1.2±0.5	1.2±0.5	-	Trace (<1)	Trace (<1)
Plagioclase feldspar	-	26.2±0.6	28.2±0.6	-	20.4±0.8	22.4±0.8
Amorphous phase	63.4±2.1	29.2±3.0	27.0±3.0	55.7±2.1	19.0±3.0	17.0±3.0

Thermal treatment at 800 and 1000 °C was also carried out on the 30_A and 40_A samples and relevant mineralogical phases are reported in Table 4.

As previously experienced in the matrix (0_A), after heating up to 800 °C for 2 h, a reduction in the amorphous phase content compared to the as-cured materials is verified in both cases (30_A and 40_A). Plagioclase feldspar is found in both 30_A and 40_A as the predominant new crystalline phase in accordance with that obtained for 0_A. In addition, the 30_A sample exhibits small amounts (< 2 wt%) of crystalline nepheline, which is present only in traces amounts in the 40_A sample.

It is assumed that the crystalline phases are formed as a consequence of a partial crystallization of the amorphous aluminosilicate gel. No further significant changes in the mineralogical composition of the composites are found after the thermal treatment at 1000 °C.

Even if some authors have reported a detrimental effect on the properties of AAMs linked to feldspar crystalliza-

tion [18], in other cases, the presence of this new phases is considered beneficial to their performance [34,35]. To verify this effect, the residual compressive strength of the 40_A cubic specimens after thermal treatment at 800 and 1000 °C was assessed. The obtained results, reported as an average of two measurements, confirm a positive effect of the plagioclase feldspar crystallization. Indeed, the compressive strength is equal to 44.6 ± 7.8 and 50.7 ± 0.3 MPa in the case of exposure to 800 and 1000 °C, respectively. These values represent a six-fold increase in compressive strength compared to the same composite (40_A) cured at room temperature, which was characterized by a compressive strength of 8.0 ± 0.8 MPa. Therefore, the phase composition changes owing to the amorphous into crystalline transition are responsible for the determined improvement in the mechanical performance of the composite.

Fig. 5 shows the mass loss, density, and water absorption of the composites after thermal treatment as a function of the RRP content and curing condition. The black bars represent the composites' mass loss after they had been dried at 105 °C for 24 h to measure the relevant bulk density and water absorption (also reported in black). Generally, the heat-induced mass loss, density, and water absorption variations of the composites follow the same trend of the relevant matrix (Table 3). Also in the case of the composites, the substantial variation in mass is verified during drying at 105 °C, and it mainly concerns the composites cured at room temperature. Moreover, regardless of the RRP content, an increase in density as well as a decrease in the water absorption values are found after exposure to 800 and 1000 °C. Both the density increase and reduction in porosity validate the increase in compressive strength determined in the 40_A sample after the thermal treatment.

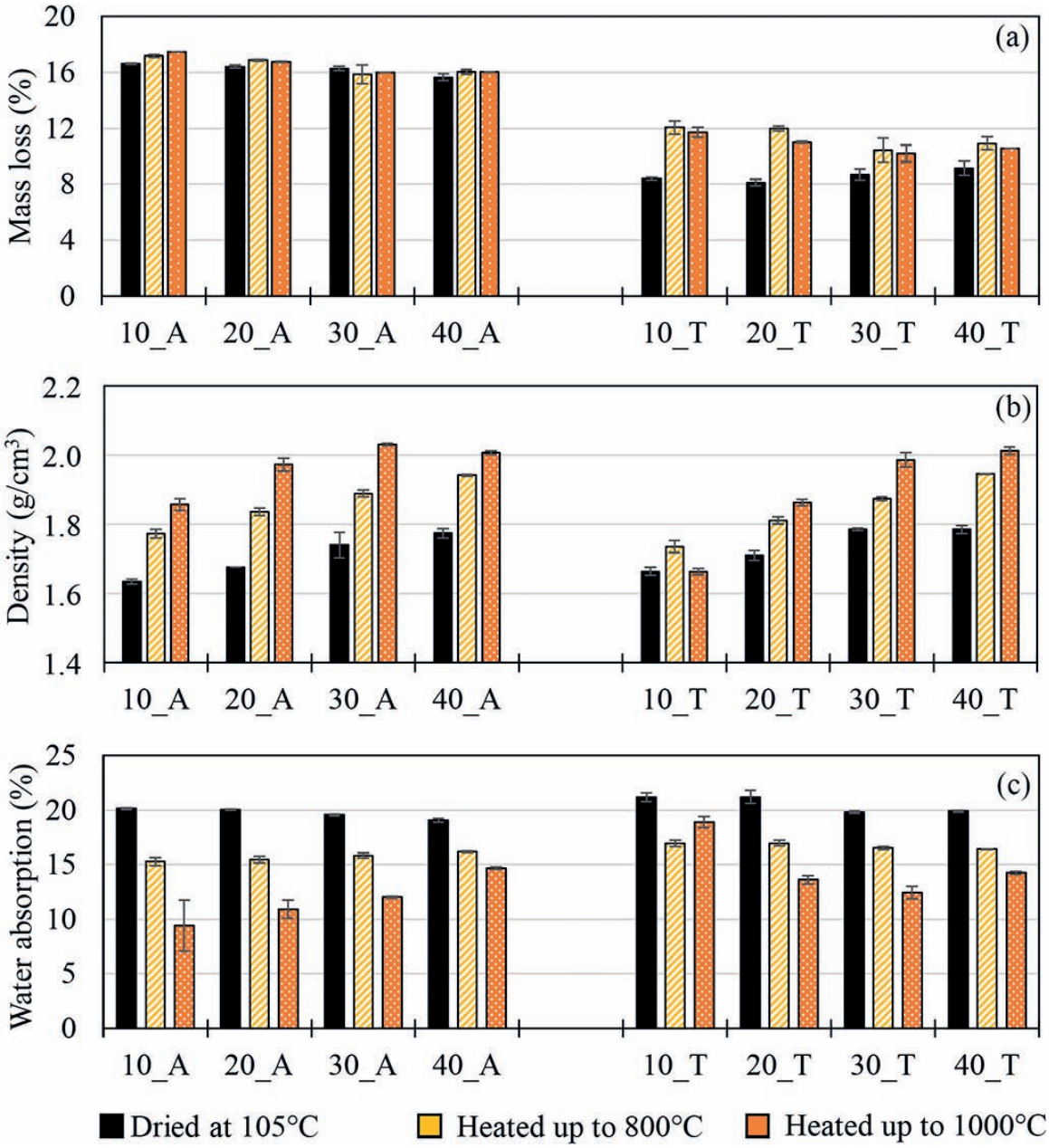

Fig. 5: Quantification of mass loss (a), density (b) and water absorption (c) of the composites after drying (T = 105 °C) and thermal treatment (T = 800 and 1000 °C).

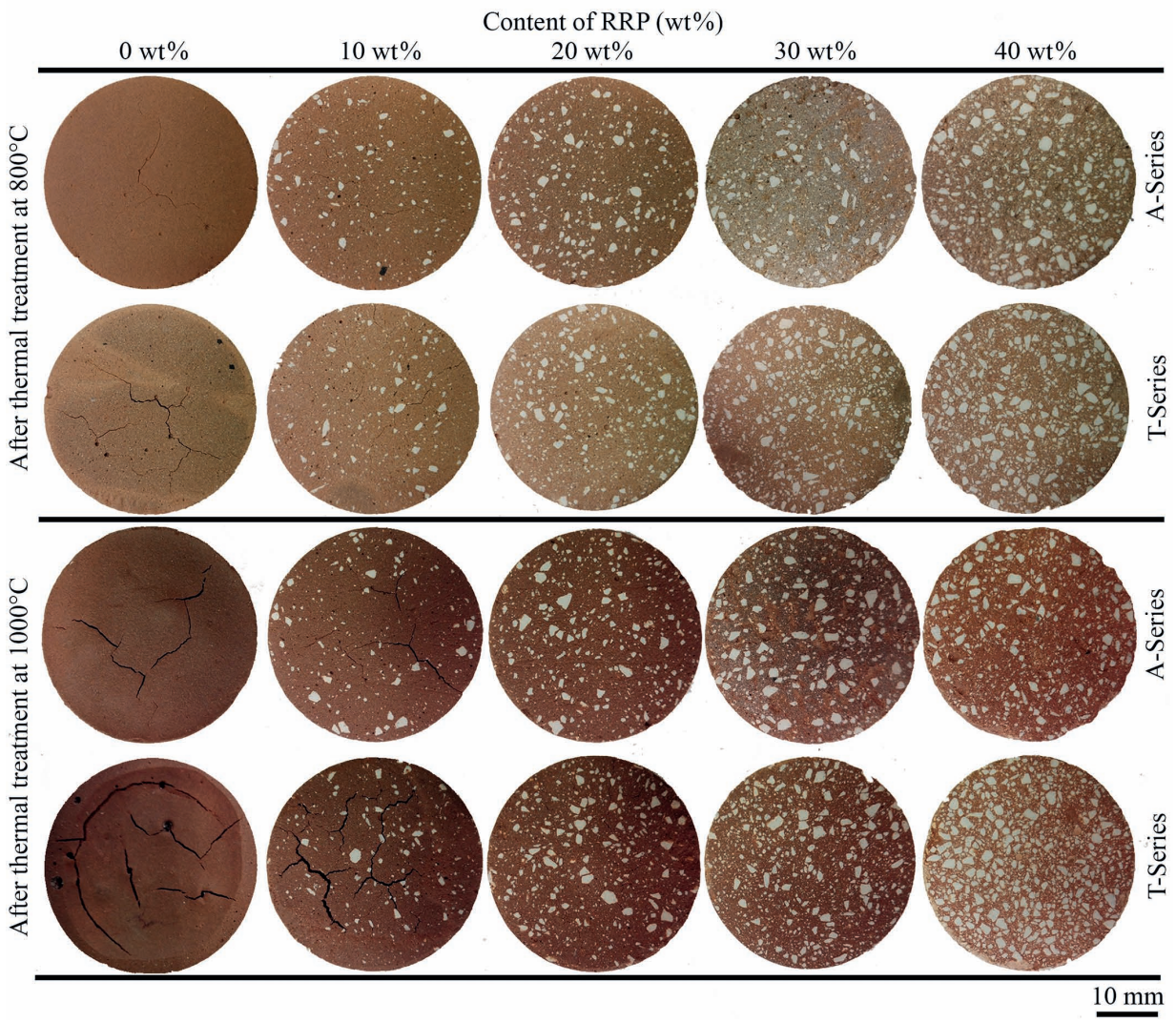

Fig. 6: Pictures of the specimens after thermal treatment at 800 °C (upper rows) and 1000 °C (lower rows).

Sample 10_T shows a slight decrease in density and an increase in water absorption after thermal treatment at 1000 °C owing to the occurrence of significant cracking followed by volumetric expansion. Such behaviour was also found for the relevant 0_T matrix as previously described, but it was not detected for a content of RPP ≥ 20 wt%, thus indicating that a proper content of dispersed phase can prevent severe cracking when heat-curing is performed. The heat-induced cracking will be further investigated in Section III(3).

Finally, the introduction of RRP is beneficial in terms of mass stability, generally leading to a lower mass loss compared to the relevant matrix. Indeed, composites containing 40 wt% RRP show a mass loss of 16.0 % (40_A) and 10.6 % (40_T) after exposure to 1000 °C (Fig. 5), whereas the mass loss of the relevant matrices are equal to 19.3 % (0_A) and 14.8 % (0_T) as shown in Table 3.

(3) Qualitative observations on the composites and investigation of their thermal dimensional stability

Fig. 6 shows images of the specimens after thermal treatment at both 800 and 1000 °C. Changes in the samples' colour from a grey to reddish colour and more intense red when heated at 800 and 1000 °C, respectively, are clearly observed. This phenomenon is common in fly-ash alkali-activated materials and it is usually related to the oxidation of the iron species contained in the fly ash [12, 35].

Crack formation due to the thermal treatment is also visible in the images. The matrices (0_A and 0_T samples) exposed to both 800 and 1000 °C present macro-cracks (width ≤ 0.6 mm, with more severe damage when heat curing is performed. As previously discussed, the curing conditions affect the pore size distribution of the matrices. Indeed, in heat-cured samples, which are characterized by a structure richer in smaller pores, a stronger capillary pressure during dehydration is probably responsible for the greatest damage. It remains unclear whether the crack formation occurs only during heating or there is also a contribution to cracking during the cooling process, as suggested by some authors [36]. Additional investigations are in progress to clarify this issue.

The use of RRP proved to be a possible solution to avoid cracking. In fact, regardless of the curing conditions, the presence of the particulates favours the progressive reduction of cracking (Fig. 6). When exposed to 800 °C, 20 wt% RRP is sufficient to guarantee the integrity of the material. However, when the temperature of exposure is increased up to 1000 °C, the integrity of the samples

is maintained only in specimens cured at room temperature (Fig. 7). Composites containing 30 wt% and 40 wt% RRP appeared undamaged after both thermal treatments regardless of the curing condition adopted (Fig. 7).

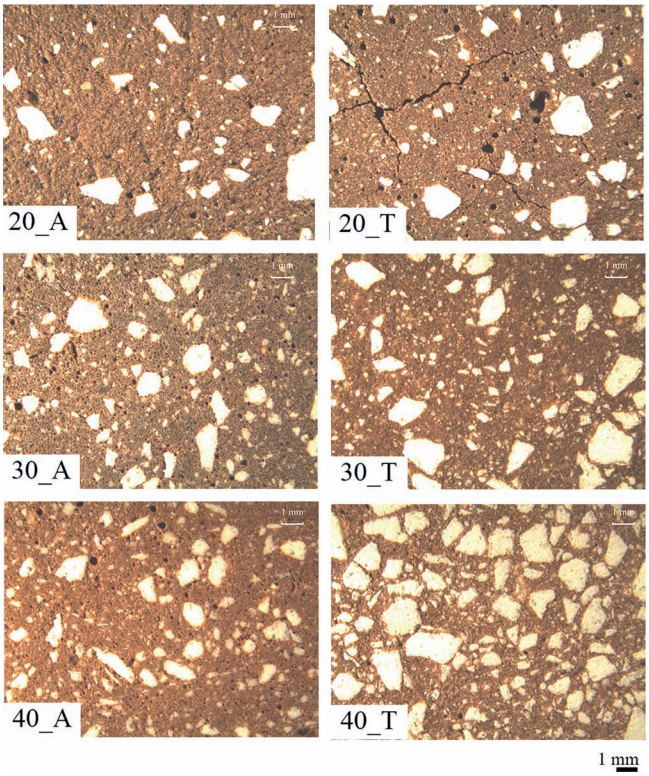

Fig. 7: Optical micrographs (10X) of composites containing 20, 30, and 40 wt% RRP, after thermal treatment at 1000 °C.

Heating microscope analysis and dilatometry were used to investigate more precisely the thermal dimensional stability of the developed composites.

The heating microscope analysis allows observation of the geometrical modification of the samples during heating at a constant rate of 5 K/min up to the complete melting of the material (Fig. 8a). In this way, it is possible to identify the temperature above which the material undergoes significant geometrical modification, which is therefore considered the maximum temperature of its thermal dimensional stability (T_{max} in Fig. 8b). For the sake of brevity, only some of the images obtained with the heating microscope are shown in Fig. 8a. Generally, geometrical thermal stability up to 1000 °C is determined and it is not significantly influenced by the curing conditions.

In particular, the 0_A and 0_T samples show reversible expansion between 600 and 850 °C and stability up to 1140 °C. When 10 wt% and 20 wt% RRP are added, T_{max} increases up to 1170 °C (10_A and 10_T) and 1200 °C (20_A and 20_T), respectively. Samples 30_A and 30_T are stable up to 1225 °C and 1240 °C, respectively. In all the aforementioned cases, above the maximum temperature of stability a swelling of the samples is detected. Finally, the specimens containing the highest amount of RRP considered in this research (40_A and 40_T) show stability up to temperatures in the range of 1210 – 1220 °C. In these cases, above the determined T_{max}, the specimens experience shrinkage before swelling.

According to the presented findings, the use of RRP up to the amount of 30 wt% appears to be effective in increasing the temperature range of dimensional stability of the studied FA-AAMs. Above this amount, the effectiveness of the particulates is no longer substantial. Moreover, from the heat curing, no interesting benefits in terms of dimensional stability at high temperature are found that could justify the additional costs of this curing condition.

In order to better investigate the dimensional stability of the composites, the dimensional changes during heating up to 1000 °C were assessed *in situ* with a dilatometer. On the basis of the previous results, the focus was on room-temperature-cured samples (0_A, 10_A, 30_A, and 40_A). The results are consistent with the heating microscope analysis since all samples show high dimensional stability up to 1000 °C with dimensional changes of ± 2 % (Fig. 9). The curves are also consistent with the thermal expansion and shrinkage of low-calcium-based alkali-activated materials, extensively investigated in the literature [33, 37 – 39]. After the dehydration shrinkage recorded in the temperature range of 110 – 230 °C, all samples show stability up to above 530 °C. The dehydration identified based on mass loss measurements, which occurs for temperatures below 105 °C, does not seem to cause shrinkage. Between 530 and 640 °C, shrinkage is observed, mainly linked to a densification of the sample [12, 40]. The densification found in this range of temperature could justify the increased values of density measured after thermal treatment in the muffle furnace. The most evident difference among the investigated samples is found in the region of 660 to 770 °C. In this range of temperature, the literature does not report a clear trend in linear dimensional changes, which vary according to the material's composition. However, it is not uncommon to measure thermal expansion, as the one measured in the case of the 0_A and 10_A samples, usually linked to the bloating of residual silicate phases and/or crack formation [37, 39].

It is interesting to note that the reactions leading to the expansion are hindered or influenced by the presence of the refractory grains. Indeed, with the addition of 10 wt% refractory particles and therefore a reduction in the total amount of silicates contained in the sample, a decrease in expansion is found. Expansion disappears totally when 30 and 40 wt% RRP is used. From these results, it appears that the use of RRP can prevent both the bloating of silicate phases and crack formation, increasing the range of the thermal dimensional stability, which is characterized by a total shrinkage lower than 1 % up to 800 °C in the case of the 40_A sample. 30_A and 40_A composites present similar dimensional changes which are mainly characterized by three areas of shrinkage in the temperature ranges of 110 – 230 °C, 550 – 630 °C, and 770 – 860 °C. In the case of 30_A, dehydration shrinkage is retarded compared to 40_A and starts at a slightly higher temperature (~ 130 °C). Up to around 860 °C, the 30_A total shrinkage is higher than that of 40_A. Above this temperature, 30_A returns to being dimensionally stable, whereas 40_A undergoes further shrinkage up to 1000 °C. The shrinkage from 800 to 1000 °C may be due to the further local densification or sintering of the matrix gel.

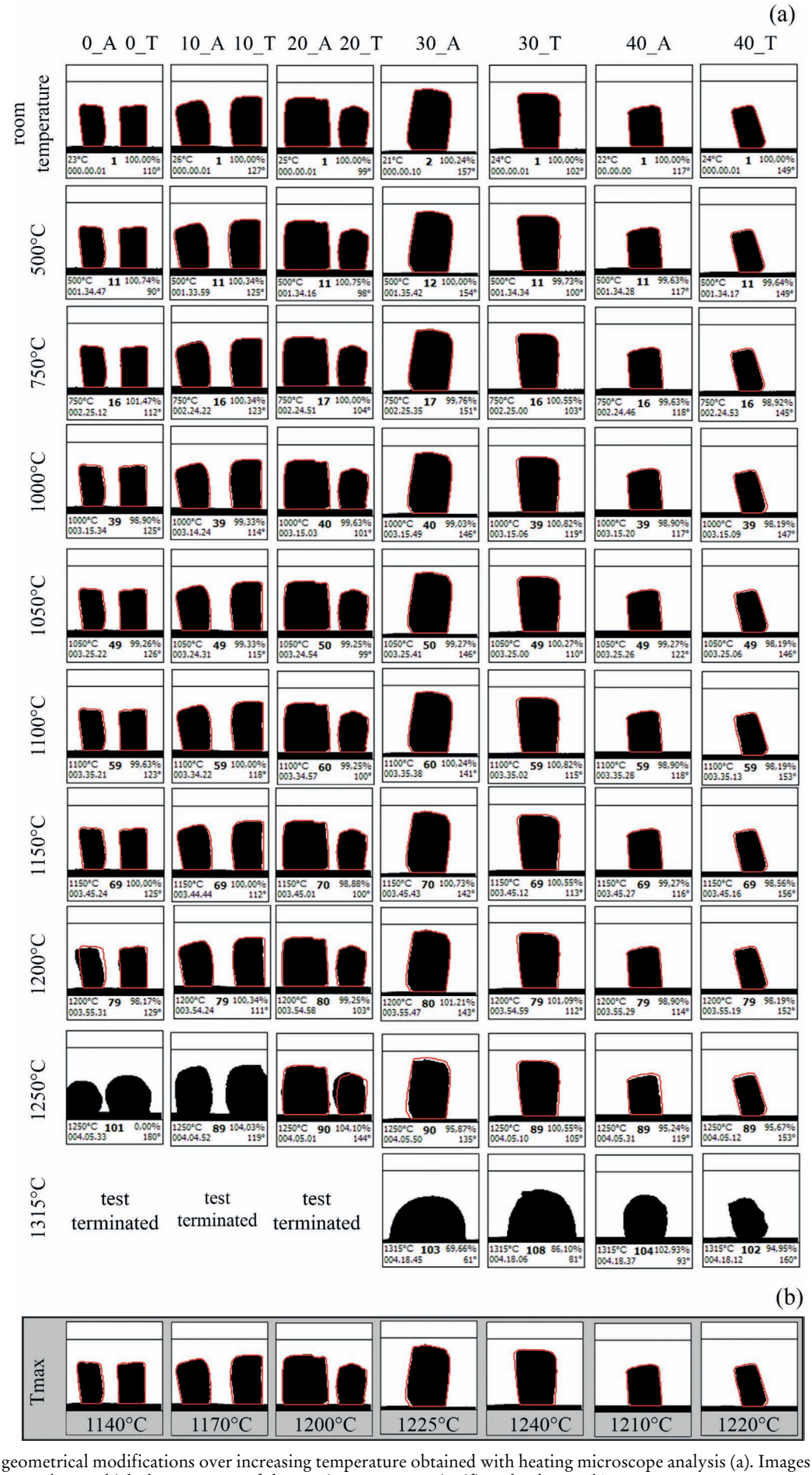

Fig. 8: Samples' geometrical modifications over increasing temperature obtained with heating microscope analysis (a). Images of the specimens at T_{max}, temperature above which the geometry of the specimen starts to significantly change (b).

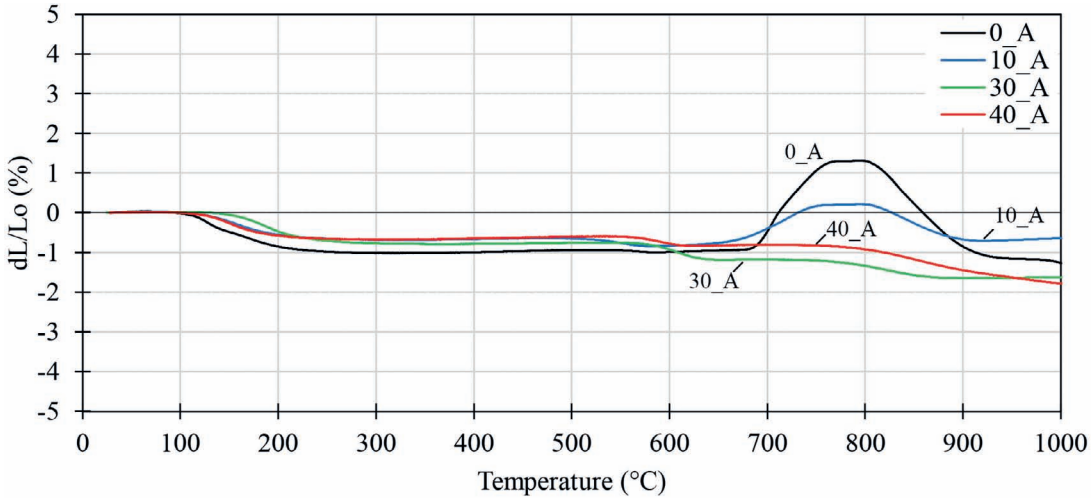

Fig. 9 : Linear dimensional changes of the 0_A, 10_A, 30_A, and 40_A samples during dilatometry measurements.

IV. Conclusions

The following conclusions can be drawn:

- After 2 h exposure to temperatures ≥ 800 °C, crystallization of plagioclase feldspar and localised sintering and densification processes occur, which result in an increase in the compressive strength of the composite;
- No significant benefits are obtained from the heat curing in terms of thermal dimensional stability. On the contrary, when exposed to high temperature, heat-cured specimens show greater cracking in the case of low amounts of dispersed RRP (0, 10, 20 wt%);
- The use of RRP improves the linear dimensional stability during heating. The use of the particles progressively reduces the expansion that occurs in the temperature range of 660 – 770 °C. The developed composites show a linear shrinkage contained in 2 % at 1000 °C;
- The inclusion of recycled refractory particles is a suitable path for improving the high-temperature performance of fly-ash-AAMs. Indeed, the use of RRP does not hinder the alkali activation process and increases the maximum temperature of dimensional stability from 1140 °C to 1240 °C. The amount of 30 wt% RRP is sufficient to inhibit the cracking after 2 h exposure to 1000 °C.

These results are promising for promoting the use of alkali-activated composite materials as innovative and sustainable products for applications requiring good dimensional stability at high temperature.

References

1 Provis, J.L.: Alkali-activated materials, *Cem. Concr. Res.*, (2017). https://doi.org/10.1016/j.cemconres.2017.02.009

2 Palomo, A., Krivenko, P., Garcia-Lodeiro, I., Kavalerova, E., Maltseva, O., Fernández-Jiménez, A.: A review on alkaline activation: new analytical perspectives, *Mater. Constr.*, **64**, 1 – 24, (2014).

3 Duxson, P., Provis, J.L.: Designing precursors for geopolymer cements, *J. Am. Ceram. Soc.*, **91**, 3864 – 3869, (2008).

4 Provis, J.L., van Deventer, J.S.J.: Geopolymers: Structures, processing, properties and industrial applications, Woodhead Publishing, Sawston, Cambridge, 2009.

5 Bernal, S.A., Krivenko, P.V., Provis, J.L., Puertas, F., Rickard, W.D.A., Shi, C., van Riessen, A.: Other potential applications for alkali-activated materials, in Alkali Activated Material, ed. by Provis J.L., van Deventer J.S.J, Springer, Netherlands, 339 – 379, 2014.

6 Natali Murri, A., Rickard, W.D.A., Bignozzi, M.C., van Riessen, A.: High temperature behaviour of ambient cured alkali-activated materials based on ladle slag, *Cem. Concr. Res.*, **43**, 51 – 61, (2013).

7 Barbosa V.F.F., MacKenzie, K.J.D.: Thermal behaviour of inorganic geopolymers and composites derived from sodium polysialate, *Mater. Res. Bull.*, **38**, 319 – 331, (2003).

8 Kong, D.L.Y., Sanjayan, J.G., Sagoe-Crentsil, K.: Factors affecting the performance of metakaolin geopolymers exposed to elevated temperatures, *J. Mater. Sci.*, **43**, 824 – 831, (2008).

9 Duxson, P., Lukey, G.C., van Deventer, J.S.J.: The thermal evolution of metakaolin geopolymers: part 2 – phase stability and structural development, *J. Non-Cryst. Solids*, **353**, 2186 – 2200, (2007).

10 Temuujin, J., van Riessen, A.: Effect of fly ash preliminary calcination on the properties of geopolymer, *J. Hazard. Mater.*, **164**, 634 – 639, (2009).

11 Zhang, Z., Provis, J.L., Zou, J., Reid, A., Wang, H.: Toward an indexing approach to evaluate fly ashes for geopolymer manufacture, *Cem. Concr. Res.*, **85**, 163 – 173, (2016).

12 Rickard, W.D.A., van Riessen, A., Walls, P.: Thermal character of geopolymers synthesized from class F fly ash containing high concentrations of iron and α-quartz, *Int. J. Appl. Ceram. Technol.*, **7**, 81 – 88, (2010).

13 Turner, L.K., Collins, F.G.: Carbon dioxide equivalent (CO_2-e) emissions: A comparison between geopolymer and OPC cement concrete, *Constr. Build. Mater.*, **43**, 125 – 130, (2013).

14 Jamieson, E., McLellan, B., van Riessen, A., Nikraz, H., Comparison of embodied energies of Ordinary Portland Cement with Bayer-derived geopolymer products, *J. Clean. Prod.*, **99**, 112 – 118, (2015).

15 Habert, G., d'Espinose de Lacaillerie, J.B., Roussel, N.: An environmental evaluation of geopolymer based concrete production: reviewing current research trends, *J. Clean. Prod.*, **19**, 1229 – 1238, (2011).

16 Kong, D.L.Y., Sanjayan, J.G., Sagoe-Crentsil, K.: Comparative performance of geopolymers made with metakaolin and fly ash after exposure to elevated temperatures, *Cem. Concr. Res.*, **37**, 1583 – 1589, (2007).

17 Zhang, H.Y., Kodur, V., Wu, B., Cao, L., Qi, S.L.: Comparative thermal and mechanical performance of geopolymers derived from metakaolin and fly ash, *J. Mater. Civ. Eng.*, **28**, 1 – 12, (2016).

18 Bakharev, T.: Thermal behaviour of geopolymers prepared using class F fly ash and elevated temperature curing, *Cem. Concr. Res.*, **36**, 1134 – 1147, (2006).

[19] Bernal, S.A., Bejarano, J., Garzón, C., Mejía de Gutiérrez, R., Delvasto, S., Rodríguez, E.D.: Performance of refractory aluminosilicate particle/fiber-reinforced geopolymer composites, *Compos. Part B Eng.*, **43**, 1919 – 1928, (2012).

[20] Musil S.S., Kriven, W.M.: *In situ* mechanical properties of chamotte particulate reinforced, potassium geopolymer, *J. Am. Ceram. Soc.*, **97**, 907 – 915, (2014).

[21] Vickers, L., Rickard, W.D.A., van Riessen, A.: Strategies to control the high temperature shrinkage of fly ash based geopolymers, *Thermochim. Acta*, **580**, 20 – 27, (2014).

[22] Kamseu, E., Rizzuti, A., Leonelli, C., Perera, D.: Enhanced thermal stability in K_2O-metakaolin-based geopolymer concretes by Al_2O_3 and SiO_2 fillers addition, *J. Mater. Sci.*, **45**, 1715 – 1724, (2010).

[23] Masi, G., Rickard, W.D.A., Bignozzi, M.C., van Riessen, A.: The effect of organic and inorganic fibres on the mechanical and thermal properties of aluminate activated geopolymers, *Compos. Part B Eng.*, **76**, 218 – 228, (2015).

[24] Ribero, D., Kriven, W.M.: Properties of geopolymer composites reinforced with basalt chopped strand mat or woven fabric, *J. Am. Ceram. Soc.*, **99**, 1192 – 1199, (2016).

[25] Natali, M.E., White, C.E., Bignozzi, M.C.: Elucidating the atomic structures of different sources of fly ash using X-ray and neutron PDF analysis, *Fuel*, **177**, 148 – 156, (2016).

[26] Bignozzi, M.C., Manzi, S., Natali, M.E., Rickard, W.D.A., van Riessen, A.: Room temperature alkali activation of fly ash: The effect of Na_2O/SiO_2 ratio, *Constr. Build. Mater.*, **69**, 262 – 270, (2014).

[27] Larson, A.C., Von Dreele, R.B.: GSAS—General Structural Analysis System. Los Alamos National Laboratory Report, LAUR, 86 – 748, 1994.

[28] Kuenzel, C., Grover, L.M., Vandeperre, L., Boccaccini, A.R., Cheeseman, C.R.: Production of nepheline/quartz ceramics from geopolymer mortars, *J. Eur. Ceram. Soc.*, **33**, 251 – 258, (2013).

[29] Rickard, W.D.A., Kealley, C.S., van Riessen, A.: Thermally induced microstructural changes in fly ash geopolymers: experimental results and proposed model, *J. Am. Ceram. Soc.*, **98**, 929 – 939, (2015).

[30] Part, W.K., Ramli, M., Cheah, C.B.: An overview on the influence of various factors on the properties of geopolymer concrete derived from industrial by-products, *Constr. Build. Mater.*, **77**, 370 – 395, (2015).

[31] Sabbatini, A., Vidal, L., Pettinari, C., Sobrados, I., Rossignol, S.: Control of shaping and thermal resistance of metakaolin-based geopolymers, *Mater. Des.*, **116**, 374 – 385, (2017).

[32] White, C.E., Provis, J.L., Proffen, T., Van Deventer, J.S.J.: The effects of temperature on the local structure of metakaolin-based geopolymer binder: A neutron pair distribution function investigation, *J. Am. Ceram. Soc.*, **93**, 3486 – 3492, (2010).

[33] Duxson, P., Lukey, G.C., van Deventer, J.S.J.: Physical evolution of Na-geopolymer derived from metakaolin up to 1000 °C, *J. Mater. Sci.*, **42**, 3044 – 3054, (2007).

[34] Rickard, W.D.A., Temuujin, J., van Riessen, A.: Thermal analysis of geopolymer pastes synthesised from five fly ashes of variable composition, *J. Non-Cryst. Solids*, **358**, 1830 – 1839, (2012).

[35] Fernández-Jiménez, A., Pastor, J.Y., Martín, A., Palomo, A.: High-temperature resistance in alkali-activated cement, *J. Am. Ceram. Soc.*, **93**, 3411 – 3417, (2010).

[36] Gluth, G.J.G., Rickard, W.D.A., Werner, S., Pirskawetz, S.: Acoustic emission and microstructural changes in fly ash geopolymer concretes exposed to simulated fire, *Mater. Struct.*, **49**, 5243 – 5254, (2016).

[37] Rickard, W.D.A., Kealley, C.S., van Riessen, A.: Thermally induced microstructural changes in fly ash geopolymers: experimental results and proposed model, *J. Am. Ceram. Soc.*, **98**, 929 – 939, (2015).

[38] Mohd Salahuddin, M.B., Norkhairunnisa, M., Mustapha, F.: A review on thermophysical evaluation of alkali-activated geopolymers, *Ceram. Int.*, **41**, 4273 – 4281, (2015).

[39] Provis, J.L., Yong, C.Z., Duxson, P., van Deventer, J.S.J.: Correlating mechanical and thermal properties of sodium silicate-fly ash geopolymers, *Colloid Surface A*, **336**, 57 – 63, (2009).

[40] Rahier, H., Simons, W., Mele, B.V., Biesemans, M.: Low-temperature synthesized aluminosilicate glasses: Part III influence of the composition of the silicate solution on production, structure and properties, *J. Mater. Sci.*, **32**, 2237 – 2247, (1997).